RSC Advances

ROYAL SOCIETY OF CHEMISTRY

www.rsc.org/advances

Synthesis of novel ammonium vanadium bronze $(NH_4)_{0.6}V_2O_5$ and its application in Li-ion battery

Yining Ma, [a,b] Shidong Ji, [a] Huanjuan Zhou, [a,b] Shuming Zhang, [a,b] Rong Li, [a] Jingting Zhu, [a,b] Wenjing Li, [a,b] Hehe Guo, [a,b] Ping Jin, [a,c,*]

[a] State Key Laboratory of High Performance Ceramics and Superfine Microstructure, Shanghai Institute of Ceramics, Chinese Academy of Sciences, Shanghai 200050, China
[b] University of Chinese Academy of Sciences, Beijing 100049, China
[c] Materials Research Institute for Sustainable Development, National Institute of Advanced Industrial Science and Technology (AIST), Nagoya 463-8560, Japan

[*] Corresponding Author at: State Key Laboratory of High Performance Ceramics and Superfine Microstructure, Shanghai Institute of Ceramics, Chinese Academy of Sciences, Shanghai 200050, China. Tel.: +86 21 69906208. Fax: +86 21 69906208.
E-mail: p-jin@mail.sic.ac.cn

Abstract

A novel ammonium vanadium bronze $(NH_4)_{0.6}V_2O_5$ has been successfully synthesized via a simple hydrothermal treatment and its electrochemical performance is investigated. The as-synthesized material was characterized by X-ray diffraction (XRD), scanning electron microscopy (SEM), transmission electron microscopy (TEM), Fourier transform infrared (FTIR) spectrum, Raman spectrum, X-ray photoelectron spectroscopy (XPS), element analysis (EA), cyclic voltammetry (CV) and galvanostatic charge/discharge cycling test. The results revealed that a pure novel phase $(NH_4)_{0.6}V_2O_5$ was obtained with square brick-like morphology. Preparation conditions such as amount of reducing agent, temperature and reaction time have been investigated to obtain the pure phase. $(NH_4)_{0.6}V_2O_5$ square bricks are tested as a cathode material for lithium-ion batteries. It has an excellent lithium ion insertion/extraction ability with a high specific discharge capacity of 280.2 mAh g^{-1} and 244.3 mAh g^{-1} during 1.0 - 3.8 V at the current densities of 10 mA g^{-1} and 20 mA g^{-1}, respectively.

Introduction

Lithium-ion batteries have been considered as attractive energy storage and conversion devices for portable electronic consumer devices, electric vehicles (EV), hybrid electric vehicles (HEV) and large-scale electricity storage in smart and intelligent grids.[1] Among diverse potential cathode candidates for lithium-ion batteries, vanadium oxides (e.g. V_2O_5, VO_2 (B), V_6O_{13}, etc.) and their derivatives have been extensively studied due to their high specific capacities, low cost, easy synthesis and wide availability on the earth.[2-5] V_2O_5 employs an orthorhombic layered structure formed from sheets of alternating pairs of VO_5 square pyramids connected by sharing corners and edges.[6] The electrostatic interactions between the layers are so weak that it is available for cations to intercalate in the interstitial sites. Insertion of cations results in the change of the V_2O_5 framework to different extents depending on the size, charge and polarizability of the cations and also generates vanadium bronze phase $M_xV_2O_5$ without a far-reaching restructuring.[6-8] It has been reported that when V_2O_5 is intercalated by electron-donating cations, the electronic conductivity will be improved.[9, 10] This endows $M_xV_2O_5$ with the special characteristic of being mixed conductors, exhibiting both ionic and electronic conductivity.[5] Such a distinctive feature makes $M_xV_2O_5$ an ideal candidate as the electrode material for electrochemical cells, potentially being fully reversible to both ions and electrons.[5] As a consequence, lots of works have been done to synthesize vanadium oxide bronzes for electrochemical properties in recent years. Fang et al. synthesized $K_{0.25}V_2O_5$ by sol-gel method and the electrodes showed superior long-term cycling stability up to 500 cycles and high specific capacity as well as good rate capability, which was better than most of previously reported performance of the metal vanadium oxides.[11] Flake-like β-$Na_{0.33}V_2O_5$ also demonstrated a high specific discharge capacity of 339 and 226 mAh g^{-1} when they worked at the current densities of 20 and 300 mA g^{-1} in the potential range of 1.5-4.0V, respectively[12]. $Ag/Ag_{0.33}V_2O_5$ hybrid demonstrated an initial capacity of 220 mAh g^{-1} at 100 mA g^{-1} and after 50 cycles, 194 mAh g^{-1} was still maintained.[13] Moreover, other types of vanadium bronzes inserted alkalis and alkaline earths elements are also reported by Liang and co-workers.[14,15]

Since $NH_4V_4O_{10}$ was firstly used as cathode material in a rechargeable lithium battery[8] in 2006, ammonium vanadium bronzes have attracted considerable attention. Flake-like $NH_4V_3O_8{\cdot}0.2H_2O$ had the greatest discharge capacity of 225.9 mAh g^{-1} during 1.8 - 4.0 V and remained 209.4 mAh g^{-1} after 30 cycles. [16] Sarkar reported that $NH_4V_4O_{10}$ along with CMC/alginate binder exhibited discharge capacity of 200 mAh g^{-1} at current rate of 1000 mA g^{-1} superior to the performance of PVDF-based cathode.[17] Except for single metal vanadium bronzes, bi-cation intercalated $(NH_4)_{0.26}Na_{0.14}V_2O_5$[18] and $(NH_4)_{0.83}Na_{0.43}V_4O_{10}{\cdot}0.26H_2O$ flowers[19] have also been obtained through hydrothermal treatment and functioned as stable lithium battery electrodes. From the above, we conclude that vanadium oxide bronzes have a variety of types and structures and are potential for rechargeable lithium-ion batteries. It would be of great significance to prepare novel structured vanadium bronze with excellent electrochemical properties to enhance competitiveness among the wide range of cathode materials world.

Herein, we report a new brick-like ammonium vanadium bronze $(NH_4)_{0.6}V_2O_5$ by hydrothermal reduction of NH_4VO_3 in an acidic solution. In order to obtain the pure phase, preparation conditions, such as amount of reducing agent, temperature and reaction time, have been optimized. The electrochemical properties of $(NH_4)_{0.6}V_2O_5$ were investigated by means of galvanostatic charge-discharge cycling and cyclic voltammetry.

Experimental

Synthesis of $(NH_4)_{0.6}V_2O_5$

Single phase $(NH_4)_{0.6}V_2O_5$ was synthesized by the hydrothermal method. All reagents were bought from Sinopharm Chemical Reagent Company and used as received. In a typical procedure, 0.4 g formic acid (HCOOH, AR) was dissolved in 40 ml deionized water, and then 1.8 g ammonium vanadate (NH_4VO_3, AR) was added into the solution under stirring at room temperature for 20 minutes. After that, the mixture was transferred into a 100 ml Teflon-lined stainless-steel autoclave (the Teflon could withstand heat up to 300 ^oC), sealed and maintained at 240-270 ^oC for 4-24 h at a heating rate of 5 $^oC\ min^{-1}$ in an electric oven . After the hydrothermal treatment, the autoclave was cooled to room temperature and the precipitate was collected by vacuum filtration, washed with distilled water and ethanol three times and then dried in vacuum at 80^oC.

Sample characterization

The crystallographic phase analysis was characterized by X-ray diffractometer (Rigaku D/Max 2550V) with Cu-Kα radiation (λ = 1.5418 Å) in the 2ϑ range from 10 ^{o} to 80 ^{o}. The morphology, microstructure and composition of samples were determined by scanning electron microscope (SEM; S-3400, HITACHI) and transmission electron microscope (TEM; JEM-2100F, JEOL) with an energy-dispersive spectrometer (EDS) attachment. Fourier transform infrared (FTIR) spectrum was recorded on a Thermo Nicolet iS10 Fourier spectrometer in the region of 400 -4000 cm^{-1} with a resolution of 4 cm^{-1}. Raman spectrum was collected on a Horiba Lab-Ram iHR550 spectrometer. The excitation light source was an argon-ion laser with λ = 632 nm. X-ray photoelectron spectroscopy (XPS) measurements were performed with a ESCALAB 250 X-ray Photoelectron Spectrometer (XPS) Microprobe with an Al Kα source. A Vario EL elemental analyzer was used for elemental analysis of nitrogen.

Electrochemical characterization

The electrochemical performance of $(NH_4)_{0.6}V_2O_5$ powders were tested as cathodes in cells and lithium foil as the anode. The composite positive electrode was consisted of the active material, conductive material (super-pure carbon) and binder polyvinylidene difluoride (PVDF) in a weight ratio of 7:2:1. The electrolyte was 1 M $LiPF_6$ in a mixture of ethylene carbonate (EC), ethyl methyl carbonate (EMC) and dimethyl carbonate (DMC) with the volume ratio of 1:1:1. The cells were assembled in an argon-filled glove box and tested on a Land CT2001A battery test system with galvanostatic charge-discharge cycling in the voltage range of 1.0 - 3.8 V. Cyclic voltammetry (CV) measurement was performed with an electrochemical workstation (CHI 604E) at a scan rate of 0.1 mV s^{-1} over the potential region of 3.8 - 1.0 V. All the tests were carried out at room temperature.

Results and discussion

Sample characterization

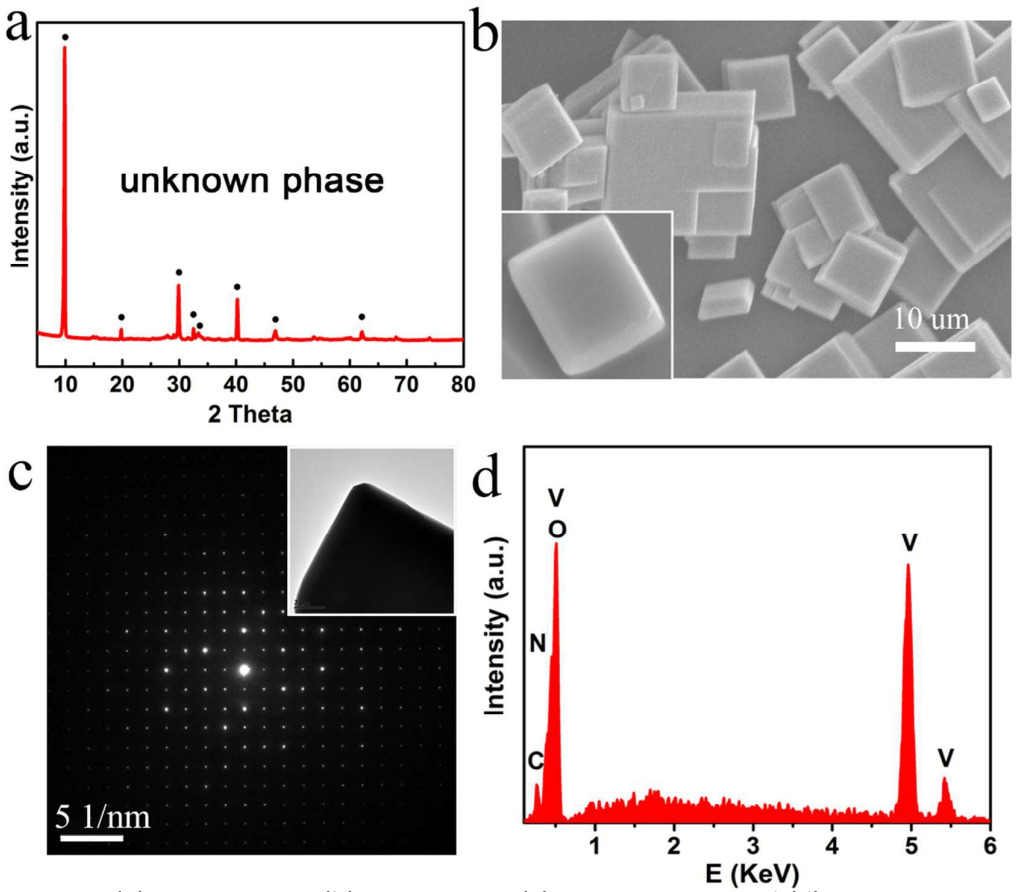

Figure 1. (a) XRD pattern, (b) SEM image, (c) SAED pattern and (d) EDS spectrum of the obtained powder by hydrothermal method.

The novel ammonium vanadium bronze was synthesized via a simple hydrothermal method with NH_4VO_3, formic acid and deionized water at 250 ^{o}C for 8 h as mentioned in the experimental section. **Fig. 1a** shows the X-ray diffraction (XRD) pattern of as-synthesized powder, all its diffraction peaks could not be ascribed to any known vanadium compounds (V_4O_9, $(NH_4)_2V_4O_9$, V_2O_5, VO_2 and vanadium oxide hydrate) to our best knowledge. The number of diffraction peaks is too few to analyze and refine the structure of product, accurately. A lot of work need to be done to solve the problem of structural analysis in the future. The morphology of the sample is square bricks with uneven sizes as shown in **Fig. 1b**. The SEM image displays that the minimum and maximum width of the square brick-like particle is about 2 and 18 um, respectively. At the same time, smooth and clean surface is observed.

In **Fig. 1c**, the selected area electron diffraction (SAED) pattern taken from one square brick indicates that it is single crystalline. The element composition of the square brick was investigated by energy-dispersive spectrometer (EDS) (**Fig. 1d**). The result shows the product contains the elements of N, V and O. To further confirm the undiscovered compound, we carried out FT-IR, Raman spectrum and XPS measurements.

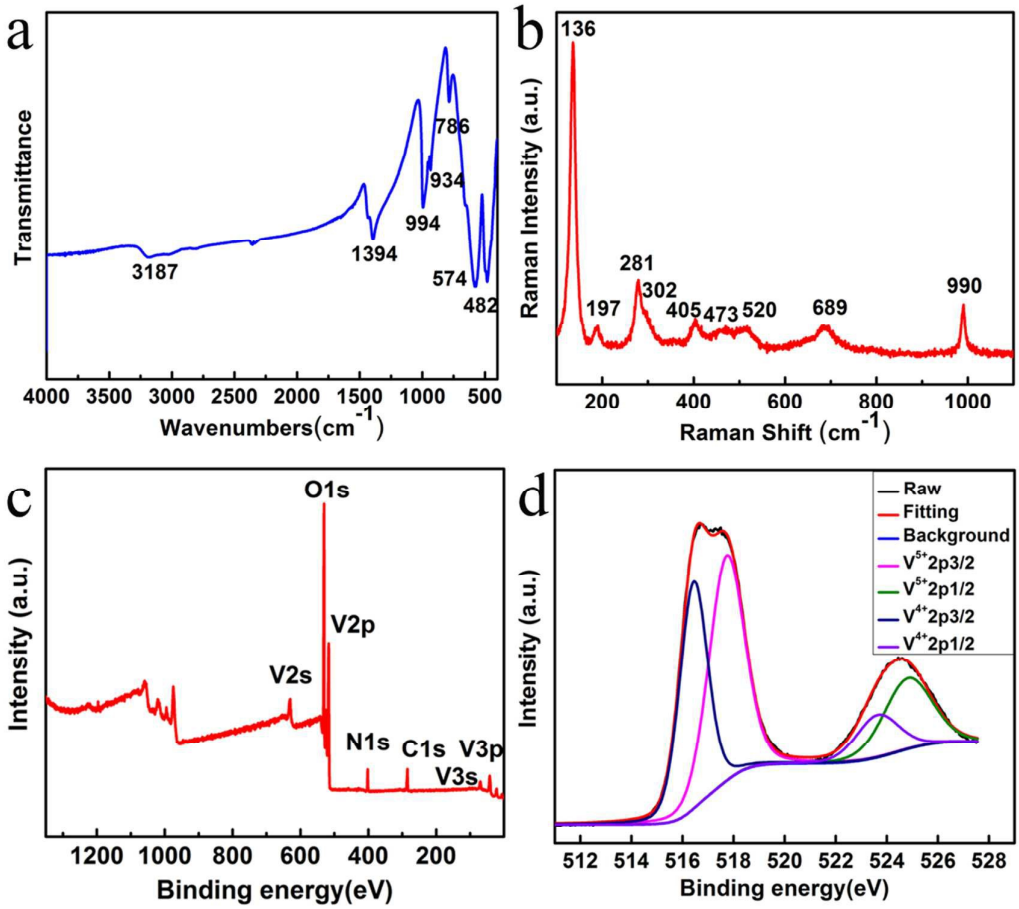

Figure 2. (a) FT - IR spectrum, (b) Raman spectrum, (c) Wide survey XPS spectrum and (d) V 2p spectrum of the as-synthesized sample.

The FT-IR spectrum of the obtained powder is shown in **Fig. 2a**. The absorption bands at ~ 3187 and ~ 1394 cm^{-1} are assigned to asymmetric stretching vibration and symmetric bending vibration corresponding to the N-H mode of NH^{4+} group.[20] The bands at ~ 994 and ~934 cm^{-1} are attributed to V=O stretching of distorted octahedral and distorted square-pyramids[21], while those at ~ 786, ~ 574 cm^{-1} and ~ 482 cm^{-1}can be contributed to asymmetric and symmetric stretching vibration of V-O-V bond, respectively.[17,22] The spectrum does not exhibit the adsorption bands at ~ 3434 cm^{-1} and ~ 1625 cm^{-1} which correspond to the O-H stretching vibration and bending vibration of the crystal water[19], inferring that it is a pure phase without water of crystallization.

To further identify the obtained phase, we carried out Raman scattering. As is shown in **Fig. 2b**, Raman spectrum exhibits a series of bands at 136, 197, 281, 302, 405, 473, 520, 689, and 990 cm^{-1}, which are well consistent with those of V_2O_5.[23,24]. The peak at 990 cm^{-1} is assigned to the stretching mode of vanadyl oxygen indicating the attainment of V_2O_5 characteristic mode.[25] The bands at 689 cm^{-1} and 520 cm^{-1} are attributed to the stretching vibrations of doubly coordinated oxygen ($V\text{-}O^2$) and triply coordinated oxygen ($V\text{-}O^3$), respectively.[26] The peaks at 405 and 281 cm^{-1} are assigned to V=O bending modes and the bands at 473 and 302 cm^{-1} belongs to V-O-V bending modes.[26] While the other two peaks recorded at 136 and 197 cm^{-1} correspond to the lattice vibration of $[V_2O_5]$.[26] From the results of unknown XRD, single crystalline SAED pattern, EDS, Raman scattering and FT-IR spectrum of the obtained sample, we conclude that the compound is an undiscovered type of

ammonium vanadium bronzes and its chemical formula is $(NH_4)_xV_2O_5$.

To further confirm the oxidation state of vanadium in the as-synthesized product, X-ray photoelectron spectroscopy measurements were carried out and the results were exhibited in **Fig. 2c** and **2d**. The wide survey XPS spectrum implies that the surface of prepared sample consists of N, V and O, which is consistent with the conclusion from EDS in **Fig. 1d**. The XPS spectrum of the V $2p^{3/2}$ peak in **Fig. 2d** is composed of two peaks at 516.5 and 517.7 eV, corresponding to V^{4+} and V^{5+}, respectively, which confirms the presence of mix-valence vanadium bronze.[25] The average valence of vanadium is +4.6 calculated from XPS data by their peak area ratios. In order to confirm the chemical formula, element analysis (EA) was performed to analyze the content of N. The result shows the weight content of N is 4.33 %. Based on the above analysis, the formula of new ammonium vanadium bronze can be expressed as $(NH_4)_{0.6}V_2O_5$. The average valance of vanadium is +4.7 calculated from the element analysis which is close to the result of XPS. Since XPS is a semi-quantitative method, the formula is subject to the result of element analysis.

Mechanism of synthesis

As mentioned earlier that vanadium oxide bronzes have a variety of types and structures due to the size, charge and polarizability of the insertion cations. At the same time, the number of insertion cations is non-stoichiometric, hence the same class of vanadium bronze may have different kinds of types and structures. For example, $Na_xV_2O_5$ system includes five phases: α phase, β phase, α' phase, δ phase and τ phase with different amount of the insertion sodion which results in various crystal structures.[27] Therefore, it is necessary to investigate the synthesis mechanism and hydrothermal reaction conditions of $(NH_4)_{0.6}V_2O_5$. Preparation conditions such as amount of reducing agent, temperature and reaction time have been varied to explore the reaction mechanism and obtain the pure phase $(NH_4)_{0.6}V_2O_5$.

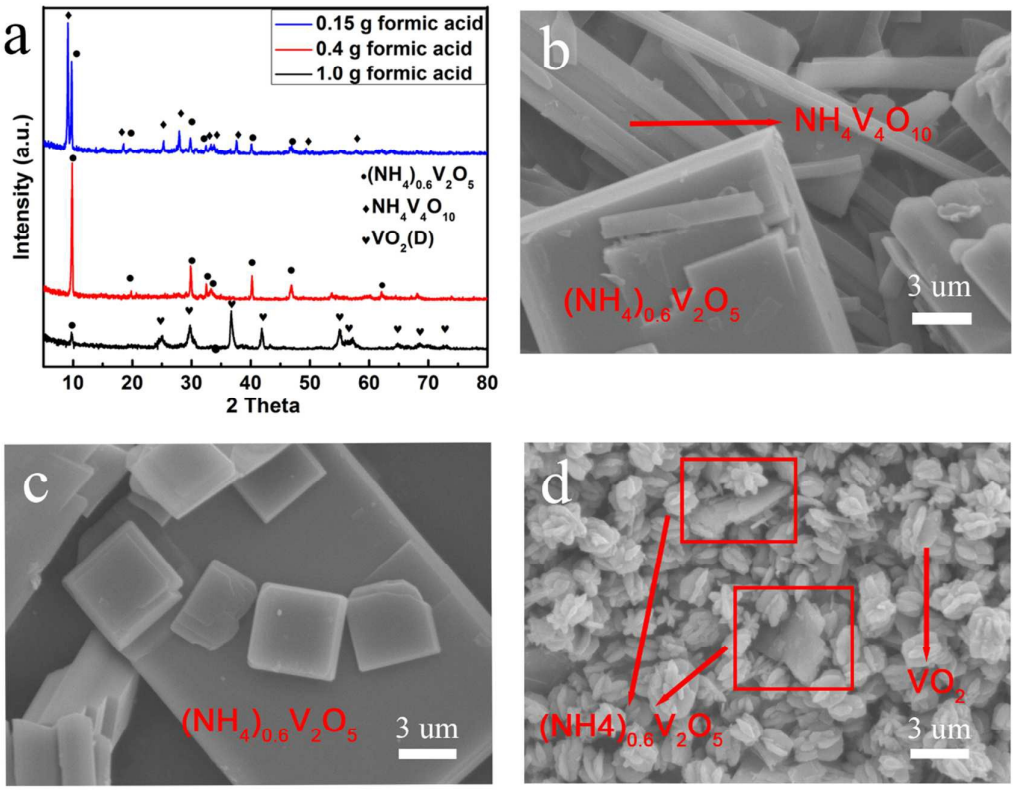

Fig. 3. (a) XRD patterns and (b - d) SEM images of hydrothermal reaction samples using different amounts of formic acid: (b) 0.15 g, (c) 0.4 g, (d) 1.0 g.

Fig. 3 shows the X-ray diffraction (XRD) patterns and scanning electron microscope (SEM) images of as-synthesized powders prepared by different amounts of formic acid assisted hydrothermal treatment. As 0.15 g formic acid was added, the final product was a mixture of $NH_4V_4O_{10}$ (JCPDS card no.31-0075) and $(NH_4)_{0.6}V_2O_5$ (**Fig. 3a**). Accordingly, the SEM image in **Fig. 3b** shows two morphologies: a nanobelt one and a square brick one, corresponding to the $NH_4V_4O_{10}$[17,28,21] and $(NH_4)_{0.6}V_2O_5$, respectively. When the formic acid was increased to 0.4 g, the pure $(NH_4)_{0.6}V_2O_5$ phase was obtained and no other impure peaks in **Fig. 3a** and morphologies in **Fig. 3c** could be observed. With further increasing to 1.0 g, the XRD pattern confirms that the powders consist of two phase $(NH_4)_{0.6}V_2O_5$ and VO_2 (D)[29]. The SEM image also identifies the $(NH_4)_{0.6}V_2O_5$ square bricks circled by red squares and VO_2 (D) micro-flowers as shown in **Fig. 3d**. $(NH_4)_{0.6}V_2O_5$ is more likely to be an intermediate phase between $NH_4V_4O_{10}$ and VO_2 (D). From the analysis above, the optimal amount of formic acid to synthesize $(NH_4)_{0.6}V_2O_5$ is 0.4 g.

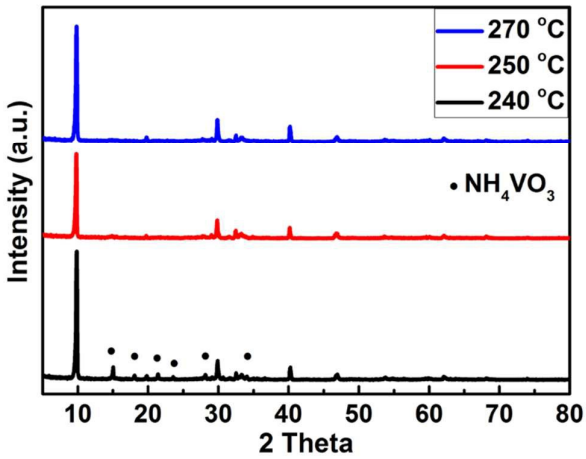

Figure 4. XRD patterns of hydrothermal reaction samples at different temperatures ranging from 240 °C to 270 °C

The reaction was also carried out at different temperatures to study the temperature effect. NH_4VO_3 could not react with formic acid completely below 250 °C even though the reaction time was 8 h, which is ascribed to the weak reducing ability of formic acid (**Fig. 4**). When the temperature reached 250 °C or higher, pure $(NH_4)_{0.6}V_2O_5$ phase was acquired. Reaction time was varied to unravel the phase evolution while the reaction temperature was kept at 250 °C (**Fig. 5**). After continuous reaction for 4 h, nanobelts $NH_4V_4O_{10}$ and square bricks $(NH_4)_{0.6}V_2O_5$ simultaneously appeared (**Fig. 5a** and **Fig. 5b**) which is similar to the consequence of less amount of the reducing agent. Pure phase $(NH_4)_{0.6}V_2O_5$ was obtained after 8 h or longer time as shown in **Fig. 5c** and **5d**. Based on the analysis above, it comes to the conclusion that the optimum condition to obtain pure phase $(NH_4)_{0.6}V_2O_5$ is that 0.4 g formic acid reacts with NH_4VO_3 at 250 °C for 8 h under hydrothermal treatment.

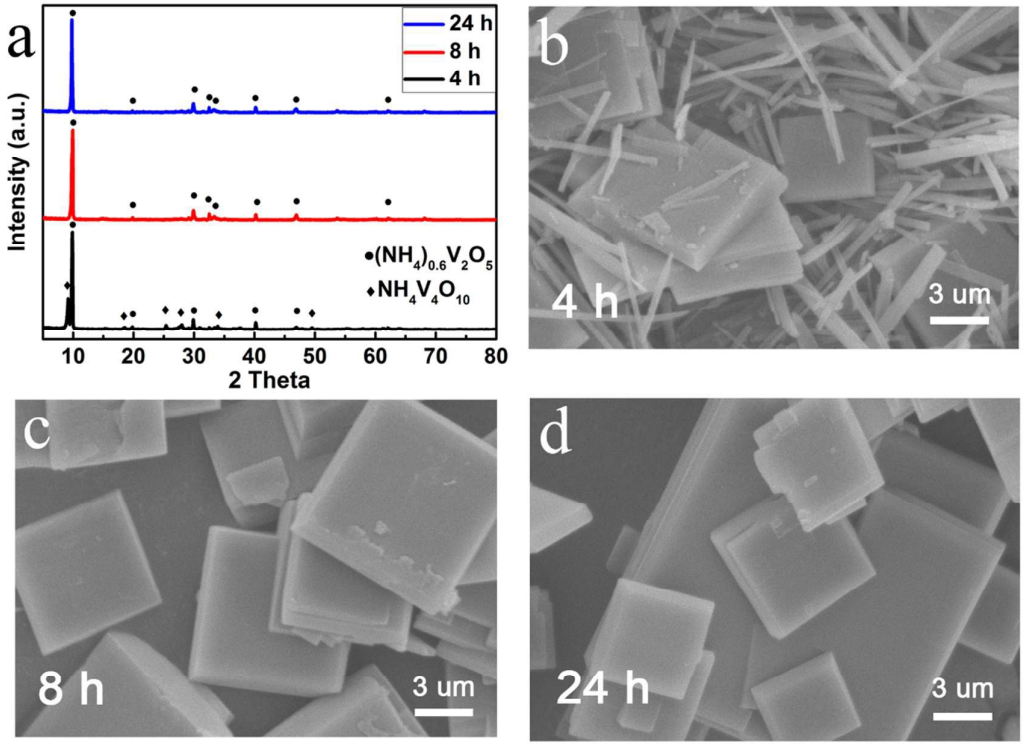

Figure 5. (a) XRD patterns and (b - d) SEM images of hydrothermal reaction samples treated under different reaction times: (b) 4 h, (c) 8 h, (d) 24 h.

Electrochemical characterization

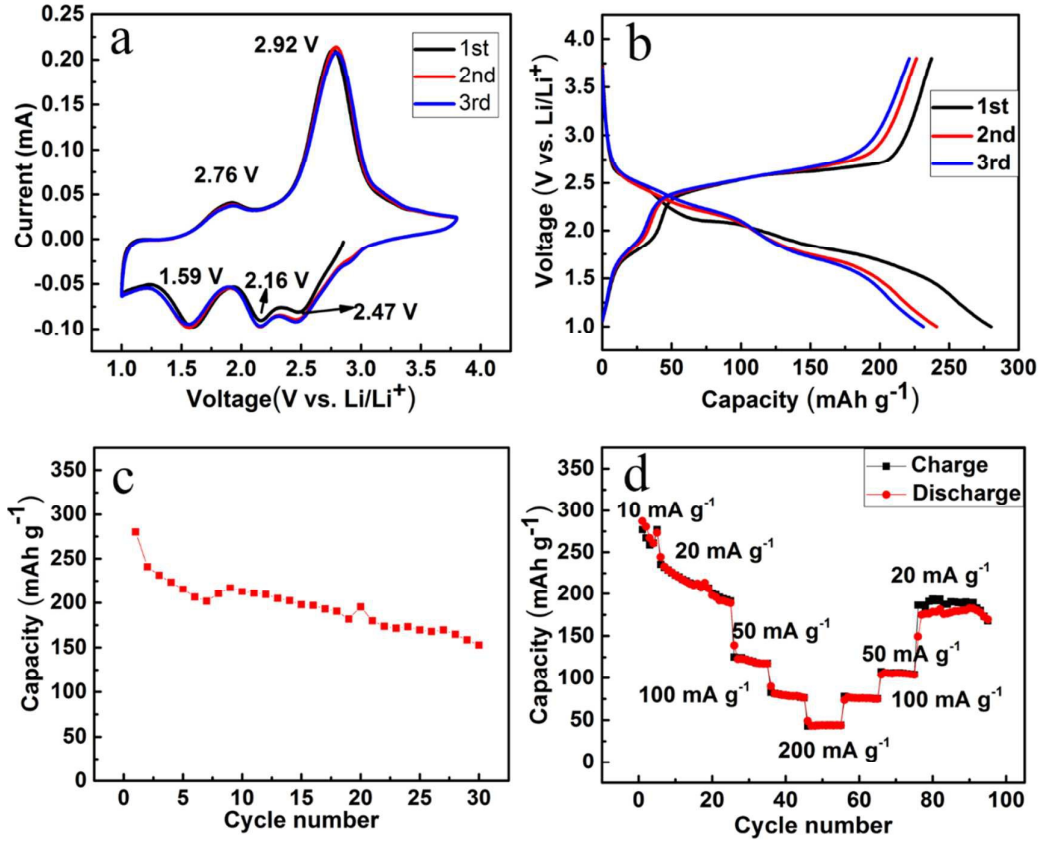

Figure 6. (a) Cyclic voltammetry curves of the square brick-like $(NH_4)_{0.6}V_2O_5$ between 1.0 and 3.8 V at a scan rate of 0.1 mV s^{-1}; (b) the first three-cycle discharge and charge profiles and (c) the cycling performance of $(NH_4)_{0.6}V_2O_5$ bricks at 10 mA g^{-1} during 1.0 - 3.8 V; (d) the rate capability of $(NH_4)_{0.6}V_2O_5$ electrode from 10-200-20 mA g^{-1}.

In order to evacuate the electrochemical performance of prepared $(NH_4)_{0.6}V_2O_5$ samples, $(NH_4)_{0.6}V_2O_5$ was adopted as the cathode material in Li-ion battery. **Figure 6a** shows typical cyclic voltammetry (CV) curves of $(NH_4)_{0.6}V_2O_5$ between 1.0 and 3.8 V at a scan rate of 0.1 mV s^{-1} for the first three cycles. In the first cycle, three reduction peaks located at 1.59 V, 2.16 V, 2.47 V and two oxidation peaks at 2.76 V and 2.92 V can be clearly identified, corresponding to the Li^+ intercalation and deintercalation process of the host material, respectively. During the latter two cycles, CVs show almost overlapping profiles, which reveal structural preservation and excellent Li^+ storage reversibility.

Figure 6b and **6c** display typical discharge/charge curves and cycling performance of $(NH_4)_{0.6}V_2O_5$ electrodes at 10 mA g^{-1} during 1.0 - 3.8 V. From **Figure 6b**, the discharge curves comprise three voltage plateaus at ~ 2.5, 2.1, and 1.6 V, which is consistent with the result of CVs, whereas the subsequent charge process exhibits S-shaped curves. Apart from the first discharge/charge curves, the other two pairs of curves show exactly similar shape, which is in good accordance with CV. It should be noted that the coulombic efficiency of the first three cycles are less than 100%. The mechanism may be more complicated, especially arising from the irreversible loss of charge capacity, which may be caused by poor electrical conductivity, the formation of solid electrolyte interface (SEI) in the first cycle, loss of some material contacting with the current collector (the structure morphology changes during Li insertion) or sluggishness of the transformation in the large particles. Moreover, the discharge curves of the second and third cycles are different from the initial discharge profile which attributed to the formation of solid electrolyte interface (SEI) with activation process and the wetting of active electrode at the beginning. Similar phenomenon has also found in other vanadium-based materials, such as $K_{0.25}V_2O_5$[11], $Ag_{0.33}V_2O_5$[30], $NH_4V_4O_{10}$[17], ect.

The galvanostatic charge/discharge cycling performance of $(NH_4)_{0.6}V_2O_5$ was shown in **Figure 6c**. It is demonstrated that the electrode can charge and discharge in the organic electrolyte, inferring that Li^+ can reversibly insert into and extract from $(NH_4)_{0.6}V_2O_5$ crystalline. The initial discharge capacity is 280.2 mAh g^{-1} and after 30 cycles, the brick-like $(NH_4)_{0.6}V_2O_5$ maintains a capacity of 152.8 mAh g^{-1}. It is worth mentioning that there is a large capacity loss during the first two cycles which is probably on account of the slight structure rearrangement stemming from the new lithium ions insertion and extraction.

Figure 6d shows the rate performance of $(NH_4)_{0.6}V_2O_5$ cathode material at varying current rates. The material delivers discharge capacity of 244.3 mAh g^{-1} at 20 mA g^{-1} which possesses a better performance than that of $NH_4V_4O_{10}$[8]. On increasing current densities from 50, 100 and 200 mA g^{-1}, capacities of 138.8, 89.8, 48.9 mA g^{-1} are obtained, respectively. It should be noted that after the continuous cycling with increasing and decreasing current densities, a specific capacity of 186.3 mAh g^{-1} could be recovered at a current of 20 mA g^{-1} which confirms the Li^+ storage

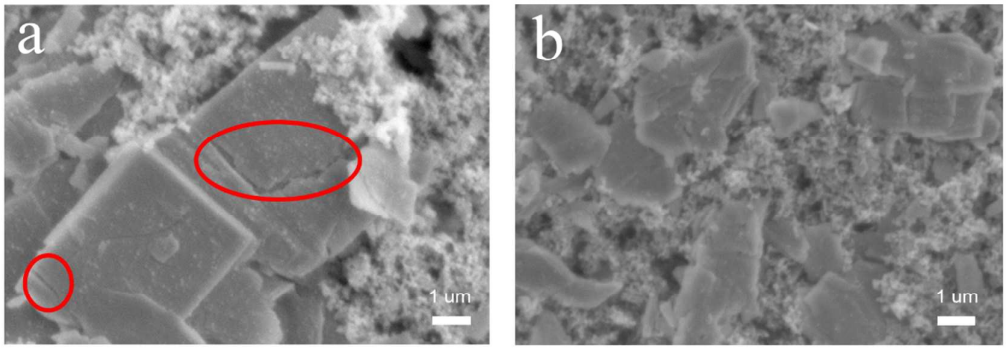

reversibility.
Figure 7. The SEM images of (NH4)0.6V2O5 electrodes, (a) after 5th cycle and (b) after 30th cycle.

From the above, we can conclude that the brick-like $(NH_4)_{0.6}V_2O_5$ exhibited a high specific discharge capacity of 280.2 mAh g^{-1} but degraded quickly after several cycles. The decay mechanism might be attributed to the structural instability of $(NH_4)_{0.6}V_2O_5$ and sluggishness of the transformation in the large particles. The capacity fading may be due to the accommodation of large amount of lithium during Li^+ intercalation and deintercalation which results in disintegration of active materials from the current collector, possibly active particle-particle contact loss or its structural collapse during long term cycling.[17] The morphology study of $(NH_4)_{0.6}V_2O_5$ electrodes after the 5th and 30th cycle are shown in Fig. 7. It can be seen in Fig. 7a that visible cracks circled by red ellipses can be clearly seen on the surface of the square bricks implying that the electrode began to disintegrate. At the same time, the surface of the bricks became rough. After the 30th cycle, the square brick disintegrated to irregular shaped pieces and the surface was wrinkled which confirms that the structural stability of $(NH_4)_{0.6}V_2O_5$ electrode is poor.

Large particle size might be another factor to cause capacity fading. Particle morphology and particle size are very important factors to determine the electrochemical performance of electrode materials.[16] Large particle would increase the Li ions' diffusion distance and make transformation sluggishness resulting in inferior electrochemical performance.

Doping heteroatoms such as Cu can not only act as pillars between layers but also stabilize the structure and improve the electronic conductivity to enhance the electrochemical performance.[2] It is expected that the fast capacity fading and bad rate capability of $(NH_4)_{0.6}V_2O_5$ electrode will be improved by doping heteroatoms.

According to the results above, it is thereby expected that as-synthesized $(NH_4)_{0.6}V_2O_5$ square brick with high specific capacity could be a promising cathode for lithium-ion battery.

Conclusion

In conclusion, we have successfully synthesized a novel brick-like ammonium vanadium bronze by means of a simple hydrothermal method. Although XRD, EDS, TEM, FTIR, Raman, XPS and EA results confirm that the obtained material is a pure phase with the chemical formula of $(NH_4)_{0.6}V_2O_5$, its crystal structure remains a mystery. To obtain the pure phase and investigate the synthesis mechanism, hydrothermal reaction conditions were studied. The electrochemical properties of $(NH_4)_{0.6}V_2O_5$ were tested as cathode in cells by galvanostatic charge-discharge cycling and cyclic voltammetry. The brick-like $(NH_4)_{0.6}V_2O_5$ exhibited a high specific discharge capacity of 280.2 mAh g^{-1} and 244.3 mAh g^{-1} during 1.0 - 3.8 V at the current densities of 10 mA g^{-1} and 20 mA g^{-1}, respectively, indicating that it could be a promising candidate as the cathode material in lithium-ion battery.

Acknowledgements

This study was financially supported by the high-tech project of MOST (2014AA032802), the Science and Technology Commission of Shanghai Municipality (STCSM, No.: 13PJ1409000, 14DZ2261200) and the National Natural Science foundation of China (NSFC NO. 51372264).

Notes and references

1. F. Cheng, J. Liang, Z. Tao and J. Chen, *Advanced materials*, 2011, 23, 1695-1715.
2. H. Yu, X. Rui, H. Tan, J. Chen, X. Huang, C. Xu, W. Liu, D. Y. W. Yu, H. H. Hng, H. E. Hoster and Q. Yan, *Nanoscale*, 2013, 5, 4937-4943.
3. X. Rui, D. Sim, C. Xu, W. Liu, H. Tan, K. Wong, H. H. Hng, T. M. Lim and Q. Yan, *RSC Adv.*, 2012, 2, 1174-1180.
4. Y. L. Ding, Y. Wen, C. Wu, P. A. van Aken, J. Maier and Y. Yu, *Nano Lett*, 2015, 15, 1388-1394.
5. N. A. Chernova, M. Roppolo, A. C. Dillon and M. S. Whittingham, *Journal of Materials Chemistry*, 2009, 19, 2526.
6. P. M. Marley, G. A. Horrocks, K. E. Pelcher and S. Banerjee, *Chem. Commun.*, 2015, 51, 5181-5198.
7. J. C. Trombe, O. Szajwaj, P. Salles and J. Galy, *J. Solid State Chem.*, 2007, 180, 2102-2109.
8. K. F. Zhang, G. Q. Zhang, X. Liu, Z. X. Su and H. L. Li, *J. Power Sources*, 2006, 157, 528-532.
9. X. C. Wu, Y. R. Tao, L. Dong and J. M. Hong, *Journal of Materials Chemistry*, 2004, 14, 901-904.
10. Y. J. Wei, C. W. Ryu and K. B. Kim, *J. Power Sources*, 2007, 165, 386-392.
11. G. Z. Fang, J. Zhou, Y. Hu, X. X. Cao, Y. Tang and S. Q. Liang, *J. Power Sources*, 2015, 275, 694-701.
12. S. Q. Liang, J. Zhou, G. Z. Fang, C. Zhang, J. Wu, Y. Tang and A. Q. Pan, *Electrochim. Acta*, 2014, 130, 119-126.
13. J. Zhou, Q. Liang, A. Q. Pan, X. L. Zhang, Q. Y. Zhu, S. Q. Liang and G. Z. Cao, *J. Mater. Chem. A*, 2014, 2, 11029-11034.
14. S. Q. Liang, J. Zhou, G. Z. Fang, J. Liu, Y. Tang, X. L. Li and A. Q. Pan, *ACS Appl. Mater. Interfaces*, 2013, 5, 8704-8709.
15. S. Q. Liang, T. Chen, A. Q. Pan, J. Zhou, Y. Tang and R. M. Wu, *J. Power Sources*, 2013, 233, 304-308.
16. H. Y. Wang, K. L. Huang, S. Q. Liu, C. H. Huang, W. J. Wang and Y. Ren, *J. Power Sources*, 2011, 196, 788-792.
17. S. Sarkar, P. S. Veluri and S. Mitra, *Electrochim. Acta*, 2014, 132, 448-456.
18. H. L. Fei, Z. R. Shen, J. G. Wang, H. J. Zhou, D. T. Ding and T. H. Chen, *Electrochem. Commun.*, 2008, 10, 1541-1544.
19. H. L. Fei, Z. R. Shen, J. G. Wang, H. J. Zhou, D. T. Ding and T. H. Chen, *J. Power Sources*, 2009, 189, 1164-1166.
20. H. A. Abbood, H. Peng, X. H. Gao, B. E. Tan and K. X. Huang, *Chem. Eng. J.*, 2012, 209, 245-254.
21. H. Wang, K. Huang, C. Huang, S. Liu, Y. Ren and X. Huang, *J. Power Sources*, 2011, 196, 5645-5650.
22. J. M. Lee, H. S. Hwang, W. I. Cho, B. W. Cho and K. Y. Kim, *J. Power Sources*, 2004, 136, 122-131.
23. J. Twu, C. F. Shih, T. H. Guo and K. H. Chen, *Journal of Materials Chemistry*, 1997, 7, 2273-2277.
24. R. Baddour-Hadjean, *Chem. Mater.*, 2008, 20, 1916–1923.
25. H. L. Fei, H. Li, Z. W. Li, W. J. Feng, X. Liu and M. D. Wei, *Dalton Trans.*, 2014, 43, 16522-16527.
26. S. H. Lee, H. M. Cheong, M. J. Seong, P. Liu, C. E. Tracy, A. Mascarenhas, J. R. Pitts and S. K. Deb, *Solid State Ionics*, 2003, 165, 111-116.

27. J. M. Savariault, J. L. Parize, D. BallivetTkatchenko and J. Galy, *J. Solid State Chem.*, 1996, 122, 1-6.
28. N. Wang, W. Chen, L. Q. Mai and Y. Dai, *J. Solid State Chem.*, 2008, 181, 652-657.
29. L. Liu, F. Cao, T. Yao, Y. Xu, M. Zhou, B. Qu, B. Pan, C. Wu, S. Wei and Y. Xie, *New J. Chem.*, 2012, 36, 619-625.
30. S. Q. Liang, Y. Yu, T. Chen, A. Q. Pan, S. D. Zhang, J. Zhou, Y. Tang and X. P. Tan, *Mater. Lett.*, 2013, 109, 92-95.